

# New Massive Binaries in the Cygnus OB2 Association

Daniel C. Kiminki<sup>1</sup>, M. Virginia McSwain<sup>2</sup>, Henry A. Kobulnicky<sup>1</sup>

## ABSTRACT

As part of an ongoing study to determine the distribution of orbital parameters for massive binaries in the Cygnus OB2 Association, we present the orbital solutions for two new single-lined spectroscopic binaries, MT059 (O8V) & MT258 (O8V), and one double-lined eclipsing binary (Schulte 3). We also constrain the orbital elements of three additional double-lined systems (MT252, MT720, MT771). Periods for all systems range from 1.5–19 days and eccentricities range from 0–0.11. The six new OB binary systems bring the total number of multiple systems within the core region of Cyg OB2 to 11. The current sample does not show evidence for a “twin-heavy” binary distribution.

*Subject headings:* techniques: radial velocities — (stars:) binaries: general — (stars:) binaries: spectroscopic — (stars:) binaries: (*including multiple*) close — stars: early-type — stars: kinematics — surveys

## 1. Introduction

The formation of massive stars is the subject of extensive debate (Krumholz 2005; Bonnell et al. 1998; Larson 2001). Current formation models are based, in part, on the accumulated statistics of massive star binary systems, such as Evans et al. (2006), Mermilliod (1995), Gies (1987), and Garmany et al. (1980). The extent to which these statistics can be generalized is limited, however, because some studies only sample small numbers of binary systems while others include large samples of systems from radically different environments with varying ages. A recent adaptive optics imaging study and modeling analysis of Sco OB2 by Kouwenhoven et al. (2007) has attempted to circumvent the selection effects of previous smaller studies in order to obtain the true binary fraction of this cluster. They find a binary fraction for B and A-type stars between 70% and 100%. Kobulnicky & Fryer (2007) utilized Monte Carlo simulations applied to the data of Kiminki et al. (2007, hereafter Paper I) to

---

<sup>1</sup>Dept. of Physics & Astronomy, University of Wyoming, Laramie, WY 82070

<sup>2</sup>Dept. of Physics, Lehigh University, Bethlehem, PA 18015

find a true binary fraction of  $f \geq 70\%$  for O and B stars in Cyg OB2. Unfortunately, the true binary fraction of massive stars in young clusters is poorly known, but it is one of several preserved parameters providing information about the formation of stellar systems. Additional parameters preserved from the formation of young binary/multiple systems are the eccentricity, separation, period, and angular momentum (in the form of rotational velocities) (Larson 2001). Understanding the initial conditions that lead to the formation of massive stars is aided by reliable statistics on a sample of binary systems sharing a common formation history. As a step toward understanding the characteristics of massive binaries in Cygnus OB2, we present a study of six new massive systems from the radial velocity survey of 150 OB stars begun in Paper I. The OB stars are probable members of the Association and lie within  $\sim 15$  pc (at  $d = 1.7$  kpc) of the cluster center surveyed by Massey & Thompson (1991). The long term goal of this study is to provide an accurate distribution of binary orbital parameters for massive stars with an assumed shared formation history.

§ 2 provides observational details of the new spectroscopic datasets. § 3 discusses the measurement of radial velocities, the search for periods in the radial velocity data, and the determination of orbital elements via radial velocity curve fitting. §4 discusses the orbital solutions to the single-lined binaries (SB1s), MT059 & MT258 (notation in the format of Massey & Thompson 1991), and the double-lined binary (SB2), Schulte 3 (Cyg OB2 no. 3). § 5 constrains the orbital elements of three additional SB2s, MT252 & MT720, and MT771. Finally, § 6 summarizes the results of the survey to date, including the total number of OB binaries uncovered in the Cyg OB2 core region.

## 2. Observations

Paper I details the observations of this survey through 2005 October. We have obtained seven additional datasets with the Longslit spectrograph on the Wyoming Infrared Observatory (WIRO) 2.3 m telescope and the Hydra spectrograph on the WIYN<sup>1</sup> 3.5 m telescope. Table 1 lists the observing runs at each facility and the corresponding spectral coverages and mean spectral resolutions. Instrumental setups at each facility for the first six runs were consistent with previous observations described in Paper I.

Observations at WIYN took place over seven nights on 2006 September 8–11 and 2007 July 3, 4, & 5. We used the Hydra spectrograph with the Red camera, 2" blue fibers, and the 1200 l mm<sup>-1</sup> grating in second order to obtain three 1200 s exposures in each of three

---

<sup>1</sup>The WIYN Observatory is a joint facility of the University of Wisconsin, Indiana University, Yale University, and the National Optical Astronomy Observatory

fiber configurations (1500–1800 s on the second run) yielding a maximum signal-to-noise ratio (S/N) of 80:1 (2006) and 130:1 (2007) for the brightest stars. The spectral coverage was 3800–4500 Å at a mean resolution of  $R \sim 4500$ . Copper-Argon lamps were used between each exposure to calibrate the spectra to an RMS of 0.03 Å (2 km s<sup>-1</sup> at 4500 Å), and the typical resolution was 1.0 Å FWHM at 3900 Å and 0.82 Å FWHM at 4400 Å. Spectra were Doppler corrected to the heliocentric frame and checked against the radial velocity standards HD182572 (G8IV), HD187691 (F8V), and the minimally varying, amply sampled star MT083 before comparison to previous datasets. Both runs were plagued by intermittent clouds.

Observations using the WIRO-Longslit spectrograph with the 600 l mm<sup>-1</sup> grating in second order took place over 12 nights from five runs of varying length (2006 June 16–20, 2006 July 15–16 & 19, 2006 October 7, and 2007 June 28–30). Exposure times varied from 600 s to 1800 s depending on weather conditions to obtain a maximum S/N of 150:1 for the brightest stars. The spectral coverage was 3900–5900 Å. Copper-Argon lamp exposures were taken after each star exposure to wavelength calibrate the spectra to an rms of 0.03 Å (1.9 km s<sup>-1</sup> at 4800 Å), and the typical spectral resolution was 2.9 Å FWHM at 4100, 2.4 Å FWHM at 4800, and 2.8 Å FWHM at 5700 (2006 October and 2007 June had a more uniform resolution of  $\sim 2.5$  Å FWHM across the chip). Spectra were Doppler corrected to the heliocentric frame and checked against the radial velocity standard HD187691 and the minimally varying, amply sampled star MT083 before comparison to previous datasets. The 2006 June and July data were affected by intermittent clouds and an abnormally high dark current arising from a camera cooling problem.

We also obtained 8 nights of spectra using the WIRO-Longslit spectrograph with the 1800 l mm<sup>-1</sup> grating in first order (2007 August 28–September 4) to examine the H $\alpha$  and He I absorption lines in suspected SB2s. Exposure times varied from 600 s to 1800 s depending on weather conditions and yielded a maximum S/N of 200:1 for the brightest stars. The spectral coverage was 5550–6850 Å and Copper-Argon lamp exposures were taken after each star exposure to wavelength calibrate the spectra to an rms of 0.03 Å (1.4 km s<sup>-1</sup> at 6400 Å). The typical spectral resolution was 1.5 Å FWHM across the chip. Spectra were Doppler corrected to the heliocentric frame and checked against the radial velocity standard HD187691 and the minimally varying, amply sampled star MT083 before comparison to previous datasets. All new datasets were reduced using standard IRAF reduction routines as outlined in Paper I.

### 3. Data Analysis and Orbital Solutions

We obtained radial velocities,  $V_r$ , for the new observations via the IRAF cross-correlation task XCSAO in the RVSAO package (Kurtz et al. 1991), using a model stellar atmosphere (Lanz & Hubeny 2003, TLUSTY) of the appropriate effective temperature and gravity as discussed in Paper I. We used the method outlined in McSwain (2003) to determine the orbital parameters of each system. We obtained an estimate of the orbital period through an IDL<sup>2</sup> program written by A. W. Fullerton which makes use of the discrete Fourier transform and CLEAN deconvolution algorithm of Roberts et al. (1987). The strongest peaks in the power spectrum of each star were examined by folding the data at the corresponding period and inspecting the  $V_r$  curve visually. Orbital elements were then procured by using the best period as an initial estimate in the nonlinear, least-squares curve fitting program of Morbey & Brosterhus (1974). The best solutions were attained by manually varying the initial guesses of key orbital parameters until a minimum in the standard deviation (*rms*) was found. Weights for each point were assigned as the inverse of the  $1\sigma$  cross-correlation velocity error, where error within the XCSAO task is calculated using,

$$\sigma_v = \frac{3w}{8(1+r)}. \quad (1)$$

In this equation  $w$  is the FWHM of the correlation peak and  $r$  is the ratio of the correlation peak height to the amplitude of antisymmetric noise (Kurtz et al. 1991).

We also included an additional  $10 \text{ km s}^{-1}$  error added in quadrature to the  $1 \sigma$  cross-correlation errors for all spectra from the 2006 June and 2006 July datasets. A varying offset of up to  $\sim 10 \text{ km s}^{-1}$  was measured for the radial velocity standard HD187691 and the amply sampled, minimally varying system MT083 during these runs. We have not been able to ascertain the source of this velocity anomaly, and we did not encounter this problem during other runs.

The complete list of orbital elements for each binary system appears in Table 2. Listed within the table are the period in days ( $P$ ), eccentricity of the orbit ( $e$ ), longitude of periastron in degrees ( $\omega$ ), systemic radial velocity ( $\gamma$ ), epoch of periastron ( $T_O$ ), primary and secondary semi-amplitudes ( $K_1$  &  $K_2$ ), adopted or calculated minimum primary and secondary masses in solar masses ( $M_1$  &  $M_2$ ), primary and secondary mass functions in solar masses ( $f(m)_1$  &  $f(m)_2$ ), spectral classifications from this survey ( $S.C._1$  &  $S.C._2$ ), the minimum primary and secondary semi-major axes in solar radii ( $a_1 \sin i$  &  $a_2 \sin i$ ), and finally,

---

<sup>2</sup>The Interactive Data Language (IDL) software is provided by ITT Visual Information Solutions.

the rms of the fits ( $rms_1$  &  $rms_2$ ).

## 4. Orbital Solutions to MT059, MT258, and Schulte 3

### 4.1. The SB1 MT059

We have accumulated 45 observations of the O8V star, MT059 (Cyg OB2 No. 1), including six at Lick, two at Keck<sup>3</sup>, eight at WIYN, and 29 at WIRO. A total of 44 spectra were included in the period search after eliminating one low S/N Lick observation. The singular peak in the CLEANed power spectrum occurs at a period of  $P = 4.852$  days. The power spectrum also contained a small amount of low power noise but no potential aliases. Figure 1 shows the  $V_r$  curve and best-fitting orbital solution with a period of  $P = 4.8527 \pm 0.0002$  days (the three most discrepant points in the figure belong to the 2006 June & July runs and were given less weight to improve the fit). Given this period, an assumed primary mass of  $M_1 = 21.4 \pm 0.6 M_\odot$  (Martins et al. 2005), and a semi-amplitude of  $K_1 = 72.3 \pm 2.3 \text{ km s}^{-1}$ , the solution yields a minimum secondary mass of  $M_2 = 5.1 \pm 0.3 M_\odot$  (where the mass error is derived from the error in the mass function). This corresponds to a mid B star or earlier (interpolated from Drilling & Landolt 2000) and a mass ratio  $q = M_2/M_1 \gtrsim 0.24 \pm 0.02$ . In the best spectra having S/N of 150:1 (WIRO-Longslit), we should be able to detect a secondary star’s spectral features at velocity separations of  $(1 + 1/q)K_1$  if the component luminosity ratio is larger than  $L_2/L_1 \simeq 0.2$  (luminosity ratios have been chosen based on a set of spectra combinations at various luminosity ratios and line separations according to spectral type and theoretical mass ratios). The absence of spectral signatures from the secondary limits the luminosity ratio to  $L_2/L_1 \lesssim 0.2$ , which, in turn, implies a secondary later than B1V and an upper limit on the mass of  $M_2 \lesssim 13.8 \pm 0.6 M_\odot$  (interpolated from Drilling & Landolt 2000). Thus, the secondary mass is constrained to  $5.1 \lesssim M_2 \lesssim 13.8 M_\odot$  and the mass ratio is  $0.24 \pm 0.02 \lesssim q \lesssim 0.64 \pm 0.03$ . The upper limit on the secondary mass also requires  $i \gtrsim 26^\circ$ , however this is a loose requirement given the uncertainty in O star masses (Massey et al. 2005). Additionally, the solution yields a minimum primary semi-major axis of  $a_1 \sin i = 6.9 \pm 0.2 R_\odot$ , an eccentricity of  $e = 0.11 \pm 0.04$ , a longitude of periastron of  $\omega = 212 \pm 17^\circ$ , and a residual  $rms = 11.0 \text{ km s}^{-1}$ . The residuals show no indication of periodicity and have a Gaussian distribution.

The ephemerides for MT059 and MT258 are listed in Table 3 and include the star

---

<sup>3</sup>The W. M. Keck Observatory is operated as a scientific partnership among the California Institute of Technology, the University of California, and the National Aeronautics and Space Administration. The observatory was made possible by the generous financial support of the W. M. Keck Foundation.

designation, date ( $HJD - 2,400,000$ ), phase ( $\phi$ ), measured radial velocity ( $V_r$ ), cross-correlation  $1\sigma$  error ( $1\sigma\ err$ ), and the observed minus calculated velocity ( $O - C$ ).

#### 4.2. The SB1 MT258

We observed another O8V star, MT258, 42 times, including two at Keck, six at Lick, 13 at WIYN, and 21 at WIRO. The six spectra obtained at Lick and one spectrum obtained at WIYN yielded low S/N and unreliable velocities with large uncertainties and were subsequently removed. The strongest signal in the CLEANed power spectrum for MT258 corresponds to a period of  $P = 14.66$  days. In addition to some low power noise, the power spectrum also contains an additional relevant signal corresponding to a period of 0.49 days. Insufficient variations over the course of a night coupled with a visual inspection of the folded  $V_r$  curve reveals this period is an alias. The  $V_r$  curve and best fitting orbital solution shown in Figure 2 ( $rms = 6.7\ \text{km s}^{-1}$ ) corresponds to a period of  $P = 14.660 \pm 0.002$  days and an orbit with an eccentricity of  $e = 0.03 \pm 0.05$ . Additionally, the orbital solution provides a semi-amplitude of  $K_1 = 41.2 \pm 1.7\ \text{km s}^{-1}$ , a primary semi-major axis of  $a_1 \sin i = 11.9 \pm 0.5\ R_\odot$ , a longitude of periastron of  $\omega = 68 \pm 71^\circ$ , and a minimum secondary mass of  $M_2 \gtrsim 4.1 \pm 0.2\ M_\odot$ , assuming a  $21.4 \pm 0.6\ M_\odot$  primary (Martins et al. 2005).  $M_2 \gtrsim 4.1 \pm 0.2\ M_\odot$  corresponds to a late-to-mid B star (interpolated from Drilling & Landolt 2000) and a mass ratio  $q \geq 0.19 \pm 0.01$ . Given the comparable S/N between MT258 and MT059 spectra, we should be able to detect a secondary star’s spectral features at velocity separations of  $(1 + 1/q)K_1$  if the component luminosity ratio is larger than  $L_2/L_1 \simeq 0.4$ . The absence of spectral signatures from the secondary and the semi-amplitude of  $K_1 = 41.2 \pm 1.7\ \text{km s}^{-1}$  limits the luminosity ratio to  $L_2/L_1 \lesssim 0.4$ , which, in turn, implies a secondary later than B0V and an upper limit on the mass of  $M_2 \lesssim 17.5 \pm 1.0\ M_\odot$  (interpolated from Drilling & Landolt 2000). Thus, the secondary mass is constrained to  $4.1 \pm 0.2 \lesssim M_2 \lesssim 17.5 \pm 1.0\ M_\odot$  and the mass ratio is  $0.19 \pm 0.01 \lesssim q \lesssim 0.84 \pm 0.05$ . The upper limit on the secondary mass also loosely requires  $i \gtrsim 18^\circ$ .

#### 4.3. The SB2 Schulte 3

Schulte 3 is listed as a probable binary system on the basis of  $H\alpha$  variability by Harries et al. (2002), and we report here the double-lined nature of this system for the first time. It is a probable member of Cyg OB2, but it lies on the outskirts of the cluster core surveyed by Massey & Thompson (1991). The spectral type of this star, O8.5IIIf (Massey & Thompson 1991, O9: in the Simbad database) is not entirely certain, and there-

fore the adopted absolute magnitude from Martins et al. (2005) is also less certain. The spectrum does carry the same diffuse interstellar band absorption (at 4428 Å and 4501 Å) characteristic of known Cyg OB2 stars (Hanson 2003). Preliminary results of a concurrent photometric survey of this cluster show this binary is also an eclipsing system with an estimated period of 4.75 days (Kinemuchi et al. 2008, in prep).

We obtained 9 exposures of this star between 2000–2007 with Hydra at WIYN, one exposure on 2000 September 19 at Keck, and eight exposures between 2007 August 28 and September 4 at WIRO with the Longslit spectrograph. The five exposures obtained at WIYN from 2006 September 8–11 show a progression from deblended, double-lined profiles to a single, slightly asymmetric profile and back. Figure 3 shows this same deblended/blended line progression in the 2007 August/September WIRO data. Using 14 of the 18 observations obtained, we deblended the He I  $\lambda\lambda 4471, 5876$  Å lines by fitting simultaneous Gaussian profiles with the SPLIT routine in IRAF to obtain rough  $V_r$  measurements. We repeated this method 10 times while varying the baseline region used to define the continuum each time. We then used the mean of each component’s list of Gaussian centers to compute the velocity and adopted the rms of this list as our one sigma uncertainty. This results in an average uncertainty of  $\leq 8$  km s $^{-1}$  for the secondary and  $\sim 20$  km s $^{-1}$  for the primary. We observe a maximum line separation of  $\sim 370$  km s $^{-1}$  for the He I lines. Emission in H $\alpha$  associated with the primary makes it difficult to compare helium with hydrogen velocities, but the maximum measured  $V_r$  separation for He I is consistent throughout the data. Based on a visual inspection of the spectra in Figure 3, a period of 4.63 days from the CLEANed power spectrum, and the preliminary results of Kinemuchi et al. (2008, in prep), we estimated a period of 4.7 days. It should be noted however, that the CLEANed power spectrum also contains a stronger signal corresponding to a period of 1.29 days, a  $1 - \nu$  alias (where  $\nu$  is the signal frequency in *days* $^{-1}$ ). However, a period of 1.29 days does not produce a sinusoidal folded  $V_r$  curve for the primary or agree with the other period estimates. We attribute the power of this signal to the considerably smaller number of data points used in the period search. The best orbital solution yields a period of  $P = 4.7464 \pm 0.0002$  days for the secondary. The period, eccentricity, epoch of periastron, and systemic velocity were applied as fixed parameters to obtain the solution for the primary. The residuals and errors are considerably higher for the primary and likely a result of emission in the helium line cores during a portion of the system’s orbit. The  $V_r$  curve and orbital solution for Schulte 3 is shown in Figure 4. The filled symbols correspond to the primary  $V_r$  measurements and the unfilled symbols correspond to the secondary  $V_r$  measurements. With a low eccentricity of  $e = 0.070 \pm 0.009$  and semi-amplitudes of  $K_2 = 256.7 \pm 2.4$  km s $^{-1}$  and  $K_1 = 113.2 \pm 14.5$  km s $^{-1}$ , the solutions yield a nearly circular orbit and a mass ratio of  $q = 0.44 \pm 0.08$ . The calculated semi-major axes are  $a_1 \sin i = 7.4 \pm 0.9$  R $_{\odot}$  and  $a_2 \sin i = 16.7 \pm 0.2$  R $_{\odot}$  (i.e., a separation of

$a \sin i = 24 \pm 0.9 R_{\odot}$ ), and the calculated lower limit masses are  $M_1 \sin^3 i = 17.2 \pm 0.3 M_{\odot}$  and  $M_2 \sin^3 i = 7.6 \pm 1.4 M_{\odot}$ . The ephemeris for Schulte 3 in Table 4 lists the star designation, date ( $HJD - 2,400,000$ ), phase ( $\phi$ ), measured radial velocities ( $V_1$  &  $V_2$ ), and the observed minus calculated velocities ( $O_1 - C_1$  &  $O_2 - C_2$ ). Errors estimates are shown in parentheses.

The top spectrum displayed in Figure 5 was obtained 2007 July 5 at WIYN. In this spectrum, the secondary’s spectral features (redshifted) are consistent with an O9III spectral type. Line ratios were estimated by a combination of equivalent width and line depth comparisons. The temperature-sensitive ratio, He I/He II  $\lambda 4026$ :He II  $\lambda 4200$  Å ( $\sim 2:1$ ), in addition to the presence of He I  $\lambda 4009$  Å, the ratio of He I  $\lambda 4144$ :He II  $\lambda 4200$  Å (1:2), and the ratio of He I  $\lambda 4471$ :H $\gamma$  & H $\delta$  (2:3) indicates the temperature class is most likely an O9 (Walborn & Fitzpatrick 1990). The luminosity indicative ratio He I  $\lambda 4026$ :Si IV  $\lambda 4089$  Å is  $\sim 2:1$  and corresponds to a luminosity class of III (Walborn & Fitzpatrick 1990). The primary’s features (blueshifted) are consistent with an O6V–III spectral type. The primary’s spectrum contains little or no evidence of Si IV  $\lambda \lambda 4089, 4116$  Å, Mg II  $\lambda 4481$  Å, or C III  $\lambda 4070$  Å indicating a temperature class O6 or earlier. The temperature-sensitive ratio, He I/He II  $\lambda 4026$ :He II  $\lambda 4200$  Å is  $\sim 1:1$  and also indicates a temperature class of O6. It is difficult to distinguish He I  $\lambda 4009$  Å from the continuum noise, but there appears to be little or no evidence of He I  $\lambda 4144$  Å, and He I  $\lambda 4471$  Å is comparatively weak. Because Si IV absorption is weak even in an O6V–III and we did not include He II  $\lambda 4686$  Å or  $\lambda 4542$  Å in our spectral coverage, the luminosity class can only be constrained to lie between III and V (interpolated from Martins et al. 2005). The bottom spectrum in Figure 5 is a composite of two spectra from the Walborn & Fitzpatrick (1990) digital atlas, HD37043 (O9III) and HD93130 (O6III). Intrinsic He I, He II, C III, Si IV, Mg II, and hydrogen absorption are labeled. We found the best agreement with Schulte 3 when HD37043 and HD93130 were combined with an equal component luminosity ratio, indicating the primary may in fact have a luminosity class of IV (interpolated from Martins et al. 2005).

There is a discrepancy between the theoretical mass ratio ( $q = 0.64 \pm 0.02$  for an O6III & O9III or  $q = 0.72 \pm 0.02$  for an O6V & O9III) obtained from Martins et al. (2005) and the mass ratio of  $q = 0.44 \pm 0.08$  found in this study. We attribute this discrepancy to either the uncertainty in mid-to-early O star masses (Massey et al. 2005), or the possibility of significant mass transfer between the components based on the hydrogen and helium emission line profiles (Miller et al. 2007; Falceta-Gonçalves et al. 2006; Sana et al. 2001). It should be noted that an uncertainty in the spectral type of each component could also partially explain the discrepancy. For instance, an O6III primary and O9.5V secondary results in a mass ratio of  $q = 0.45 \pm 0.02$  (Martins et al. 2005). However, this combination produces a luminosity ratio in disagreement with the implied luminosity ratio of the double-lined spectra and the light curve of Schulte 3. An O5III primary and O9.5III secondary would also replicate the



computed mass ratio within the error ( $q = 0.51 \pm 0.01$ ; Martins et al. 2005), but also suffers from the same luminosity ratio disagreement. A likely scenario that explains the mass ratio discrepancy may involve a combination of two or more factors. Further analysis of the light curve for Schulte 3 (Kinemuchi et al. 2008, in prep) and additional spectroscopic coverage is necessary however, to verify the presence of a mass transfer mechanism and determine what type of eclipsing system this is.

## 5. Period Estimates of three Multi-lined Systems

The 2007 August/September dataset was not sufficient to fit solutions to three double-lined systems but did allow for stricter constraints on the orbital elements. We applied the same method used for Schulte 3 to measure radial velocities for the components of these systems. Figures 6, 8, & 9 provide the time series for  $H\alpha$   $\lambda 6563$  Å and He I  $\lambda 5876$  Å in velocity space for MT252, MT720, and MT771 (2007 August 28 through 2007 September 4). Each system was introduced in Paper I with approximate periods and secondary mass estimates.

### 5.1. The SB2 MT252

For the first double-lined system, MT252, we obtained 23 observations from 1999–2007. MT252 is classified as a B1.5III in Paper I. We revise the classification slightly in this study to B2III. The primary shows weak C II/O II  $\lambda 4070$  Å, little or no Si IV  $\lambda 4089$  Å, and a ratio of Si III  $\lambda 4552$ :Si II  $\lambda \lambda 4128, 4430$  Å of over 2:1, indicating a B2 temperature class. The luminosity indicator, Si III  $\lambda 4552$ :He I  $\lambda 4387$  Å is nearly 2:1 and points to a luminosity class of III. The secondary shows an absence of Si IV  $\lambda 4089$  Å and C II/O II  $\lambda 4070$  Å, making it no earlier than B1. There is also no evidence of C II  $\lambda 4267$  Å or Si II  $\lambda \lambda 4128, 4130$  Å, indicating it is likely no later than a B2. A He I  $\lambda 4121$ :He I  $\lambda 4144$  Å ratio of nearly 1:1 and the absence of N III  $\lambda 4634$  Å and O II  $\lambda \lambda 4640, 4650$  Å absorption places the luminosity at V. We therefore conclude that the secondary is most likely a B1V.

Of the 23 observations obtained, only six are of high enough S/N to estimate He I line velocities. These velocities listed in Table 4 are relative to the heliocentric frame of rest. The largest line separation for MT252 is seen on 2007 August 28 (Figure 6), and a near reversal of spectral features is seen within the  $\sim 8$  days covered, indicating a likely period of 18–19 days. The maximum line separation in He I  $\lambda 5876$  Å is  $\sim 192$  km s $^{-1}$ , and the  $V_r$  semi-amplitudes are  $K_2 = 107 \pm 13$  km s $^{-1}$  and  $K_1 = 85 \pm 13$  km s $^{-1}$  relative to a systemic velocity of

$\gamma = -18 \pm 10 \text{ km s}^{-1}$  estimated from the 2007 August 30 and September 1 spectra (where the errors are approximated as they were with Schulte 3) indicating a mass ratio of  $q \simeq 0.8 \pm 0.2$ , in agreement with the theoretical mass ratio of  $q = 0.9$  (interpolated from Drilling & Landolt 2000). Based on a partial  $V_r$  vs. time curve of this system, the eccentricity appears low. Therefore, for an assumed circular orbit, semi-amplitudes of  $K_1 = 85 \pm 13 \text{ km s}^{-1}$  and  $K_2 = 107 \pm 13 \text{ km s}^{-1}$  on 2007 August 28, and a period of  $P \sim 18.5 \pm 0.5$  days, the calculated masses are  $M_1 \sin^3 i \simeq 8 \pm 1 M_\odot$  and  $M_2 \sin^3 i \sim 6 \pm 1 M_\odot$ . These values also imply a primary and secondary semi-major axes of  $a_1 \sin i \simeq 22 \pm 3 R_\odot$  and  $a_2 \sin i \simeq 27 \pm 3 R_\odot$ . It should be noted that these values reflect lower limits in the absence of a full orbital solution.

### 5.2. The SB2 MT720

MT720 is composed of two components of apparently equal luminosity based on the similar depth and ratios of hydrogen and He I lines, as illustrated in a small portion of the 2001 August 24 and 2001 September 9 observations in Figure 7. The top spectrum (August 24) shows a nearly complete blend while the bottom spectrum (September 9) shows the deblended state (with perhaps a slight asymmetry in the red wing of the Balmer lines). The blended spectral features seen on 2007 September 1 & 3 (*third and fifth spectra down*) in Figure 8 indicate the systemic radial velocity,  $\gamma$ , is near zero. While the quality of the data makes it difficult to estimate an exact period, September 2 & 4 (*fourth and sixth spectra down*) indicate the period is  $\sim 5$  days or less. The low S/N of the data makes it unclear whether the spectra show only two components. Therefore we applied both a two and three component model to both the hydrogen and He I lines in the attempt to deblend the spectral features. We obtained mixed results with the two-Gaussian fit (fixed widths), which provided velocity ratios varying from 0.4–0.9. Three Gaussians however, provided only slightly better fits to the data and again yielded varying velocity ratios. Therefore, we adopted the simpler two component model. The absence of He II in any of the spectra indicates that neither of the two components are earlier than about B0. The strength of He I coupled with the appearance of multi-component C III  $\lambda 4070 \text{ \AA}$  and weak or absent Mg II  $\lambda 4481 \text{ \AA}$  indicates that both are probably B2 or earlier. We therefore conclude the components lie between B0–B2 with uncertain luminosity classes.

### 5.3. The SB2 MT771

We obtained 36 observations (most low S/N) of the double system MT771. The primary is an O7V as indicated by the He II  $\lambda 4200$ :He I  $\lambda 4144 \text{ \AA}$  and He II  $\lambda 4200$ :He I  $\lambda 4026 \text{ \AA}$  ratios

of nearly 6:1 and 1:1 respectively. The ratio of He II  $\lambda 4542$ :He I  $\lambda 4387$  Å of just over 1:1 gives the luminosity class. The secondary is a probable O9V as best indicated by the temperature sensitive ratio of He II  $\lambda 4200$ :He I  $\lambda 4121$  Å ( $\sim 1:1$ ) and luminosity-sensitive ratio of Si IV  $\lambda 4116$ :He I  $\lambda 4121$  Å (just under 1:1).

Figure 9 shows blended features for H $\alpha$   $\lambda 6563$  Å and He I  $\lambda 5876$  Å on days 2, 5, and 8, suggesting periods of 1.5, 3, or 6 days. The similar He line profiles on days 1 and 3 suggest that one full period has elapsed, leaving the  $\sim 1.5$  day period as the only viable option. The August 30 (*third spectrum down*) spectrum shows a  $V_r$  separation of  $277 \text{ km s}^{-1}$  ( $-153 \pm 14 \text{ km s}^{-1}$  and  $124 \pm 13 \text{ km s}^{-1}$  relative to the systemic velocity of  $\gamma = -36 \pm 10.0 \text{ km s}^{-1}$  estimated from the 2007 September 1 spectrum) and implies a mass ratio of  $q = 0.8 \pm 0.1$ , consistent with a theoretical mass ratio of  $q = 0.68 \pm 0.02$  for an O7V ( $25.9 \pm 0.6 M_{\odot}$ ) and O9V ( $17.6 \pm 0.5 M_{\odot}$ ) (Martins et al. 2005). Assuming a circular orbit, period of 1.5 days, and minimum semi-amplitudes of  $K_1 = 124 \pm 13 \text{ km s}^{-1}$  and  $K_2 = 153 \pm 14 \text{ km s}^{-1}$  for the primary and secondary respectively, the minimum semi-major axes are  $a_1 \sin i \sim 2.6 \pm 0.3 R_{\odot}$  and  $a_2 \sin i \sim 3.2 \pm 0.3 R_{\odot}$ , and the masses are  $M_1 \sin^3 i \sim 1.8 \pm 0.2 M_{\odot}$  and  $M_2 \sin^3 i \sim 1.5 \pm 0.2 M_{\odot}$ . As with MT252, these values reflect lower limits in the absence of a full orbital solution. No evidence for interacting winds or mass transfer is seen. Therefore, using the theoretical radii of  $R_1 = 9.3 \pm 0.1$  and  $R_2 = 7.6 \pm 0.1$  (Martins et al. 2005), this system would need to have an inclination of  $i \lesssim 20^\circ$  to avoid contact. This is consistent with the low inclination necessary ( $i \sim 24$ ) to obtain the theoretical masses for an O7V and O9V.

## 6. Summary of Survey Results to Date

We have discovered the presence of six binary systems in the Cyg OB2 association as part of an ongoing survey to determine the distribution of binary orbital parameters. We presented the orbital solutions to three new systems (MT059, MT258, and Schulte 3) and constrained the orbital parameters to the three additional double-lined binaries (MT252, MT720 & MT771). Mass ratios for the six systems in this study range from  $q \geq 0.18 \pm 0.01$  for MT258 to  $q \simeq 0.8 \pm 0.2$  for MT252, and have periods ranging from  $\sim 1.5$ –19 days. Systemic velocities deviate by  $\sim 10$ –20  $\text{km s}^{-1}$  from the cluster mean of  $-10.3 \text{ km s}^{-1}$  obtained in Paper I, but they are still well within the Association’s radial velocity dispersion. These six systems more than double the number of known binaries in this cluster and bring the total number of uncovered OB binary/multiple systems in Cyg OB2 to 11. The locations of all 11 systems are shown in Figure 10. No evidence of grouping is apparent. Table 5 lists several key parameters for each system, including the star designation, photometric and/or spectroscopic binary type (*Type*), spectral classifications (*S.C.*), period (*P*), mass ratio when

available ( $q$ ), and literature references (*Ref*). Periods for all 11 systems are relatively short ( $< 22$  days) and the corresponding eccentricities are relatively small (0.03–0.11). With the exception of MT421, all systems have early companions. However, the apparent secondary mass distribution may depend on the sensitivity of the associated surveys.

Although our current sample encompasses only a small fraction of systems in Cyg OB2, we can test the limited mass ratio statistics against the hypothesis of Pinsonneault & Stanek (2006), that 45% of massive stars exist in “twin” systems with mass ratios of  $q > 0.95$ . Of the seven systems with mass ratio measurements in Table 5, we find at most one system that may be considered a possible “twin” (MT252 with  $q = 0.8 \pm 0.2$ ). If this hypothesis holds true, binomial statistics indicate the present distribution is likely only 8.7% of the time. On the other hand, if we consider  $q < 0.95$  for MT252, the present distribution is likely only 1.5% of the time. Under the Pinsonneault & Stanek (2006) hypothesis, we would expect to observe a distribution of two to four “twins” in a sample of seven objects (21.4%, 29.2%, and 23.9% respectively). Though no definite conclusions can yet be drawn about the agreement of these findings with Pinsonneault & Stanek (2006) owing to the limited number of systems available, at least in the case of Cyg OB2, a “twin” heavy binary distribution does not seem likely.

We thank the time allocation committees of the Lick, Keck, WIYN, and WIRO Observatories for granting us observing time and making this project possible. This paper has benefited greatly from the detailed review and suggestions of an anonymous referee. We are also grateful for support from the National Science Foundation through the Research Experiences for Undergraduates (REU) program grant AST-0353760 and through grant AST-0307778, and the support of the Wyoming NASA Space Grant Consortium. The work of M. V. McSwain is supported by the National Science Foundation, under grant AST-0401460 and she is also grateful for institutional support from Lehigh University. We also would like to graciously thank Sarah Bird, Georgi Chunev, Megan Bagley, Emily May, Christopher Rodgers, Karen Kinemuchi, Brian Uzpen, and Carolynn Moore for their help observing at WIRO though any weather condition.

*Facilities:* WIRO (), WIYN (), Shane (), Keck:I ()

## REFERENCES

Bonnell, I. A., Bate, M. R., & Zinnecker, H. 1998, MNRAS, 198, 93

- Contreras, M. E., Rodriguez, L. F., Tapia, M., Cardini, D., Emanuele, A., Badiali, M., & Persi, P. 1997, *ApJ*, 488, 153
- De Becker, M., Rauw, G., & Manfroid, J. 2004, *A&A*, 424, L39
- Drilling, J. S., & Landolt, A. U. 2000, in *Astrophysical Quantities*, ed. A. N. Cox (4th ed.; New York; Springer), 381
- Evans, C. J., Lennon, D. J., Smartt, S. J., & Trundle C. 2007, *A&A*, 464, 289
- Falceta-Gonçalves, D., Abraham, Z., Jatenco-Pereira, V. 2006, *MNRAS*, 371, 1295
- Fullerton, A. W., Gies, D. R., & Bolton C. T. 1996, *ApJS*, 103, 475
- Garmany, C. D., Conti, P. S., & Massey, P. 1980, *ApJ*, 242, 1063
- Gies, D. R., 1987, *ApJS*, 64, 545
- Hanson, M. M. 2003, *ApJ*, 597, 957
- Harries, T. J., Howarth, I. D., & Evans, C. 2002, *MNRAS*, 337, 341
- Hillwig, T. C., Gies, D. R., Bagnuolo, W. G., Jr., Huang, W., McSwain, M. V., & Wingert, D. W. 2006, *ApJ*, 639, 1069
- Kiminki, D. C., et al. 2007, *ApJ*, 664, 1120
- Kinemuchi et al. 2008, in prep
- Kobulnicky, H. A., & Fryer, C. L. 2007, *ApJ*, 670, 747
- Kouwenhoven, M. B. N., Brown, A. G. A., Portegies Zwart, S. F., & Kaper, L. 2007, *A&A*, 474, 77
- Krumholz, M. R., 2005, *ASPC*, 352, 31
- Kurtz, M. J., Mink, D. J., Wyatt, W. F., Fabricant, D. G., Torres, G., Kriss, G. A., & Tonry, J. L. 1991, in *Astronomical Data Analysis Software and Systems I*, ASP Conf. Ser., Vol. 25, eds. D.M. Worrall, C. Biemesderfer, and J. Barnes, p. 432
- Lanz, T., & Hubeny, I. 2003, *ApJS*, 146, 417
- Larson, R. B. 2001, *IAU Symposium*, 200, 93
- Martins, F., Schaerer, D., & Hillier, D. J. 2005, *A&A*, 436, 1049

- Massey, P., & Thompson, A. B. 1991, *AJ*, 101, 1408
- Massey, P., Puls, J., Pauldrach, A. W. A., Bresolin, F., Kudritzki, R. P., & Simon, T. 2005, *ApJ*, 627, 477
- McSwain, M. V. 2003, *ApJ*, 595, 1124
- Mermilliod, J. C. 1995, in *Information & On-Line Data in Astronomy*, ed. D. Egret, & M. A. Albrecht (Kluwer Academic Publishers, Dordrecht), 127
- Miczaika, G. R. 1953, *PASP*, 65, 141
- Miller, B., Budaj, J., Richards, M., Koubský, P., & Peters, G. 2007, *ApJ*, 656, 1075
- Morbey, C. L., & Brosterhus, E. B., 1974, *PASP*, 86, 455
- Pigulski, A., & Kolaczowski, Z. 1998, *MNRAS*, 298, 753
- Pinsonneault, M. H., Stanek, K. Z. 2006, *ApJ*, 639, 67
- Rauw, G., Vreux, J. M., & Bohannan, B. 1999, *ApJ* 517, 416
- Rios, L. Y., & DeGioia-Eastwood, K. 2004, *BAAS*, 205, No. 09.05
- Roberts, D. H., Lehár, J., & Dreher, J. W., 1987, *AJ*, 93, 968
- Romano, G. 1969, *MmSAI*, 40, 375
- Sana, H., Rauw, G., Gosset, E. 2001, *A&A* 370, 121
- Schulte, D. H. 1958, *AJ*, 128, 41
- Snow, T., Zukowski, D., & Massey, P. 2002, *ApJ*, 578, 877
- Walborn, N. R. 1973, *ApJ*, 180, L35
- Walborn, N. R. & Fitzpatrick, E. L. 1990, *PASP*, 102, 379
- Wilson, O. C. 1948, *PASP*, 60, 385
- Wilson, O. C., Abt, A. 1951, *ApJ*, 144, 477
- Wolff, S. C., Strom, S. E., Dror, D., Lanz, L., & Venn, K. 2006, *AJ*, 132, 749

Table 1. Summary of Observing Runs

Date	Observatory /Instrument	Spectral Coverage (Å)	Grating (l mm <sup>-1</sup> )	Mean Spectral Resolution (Å)	Date Coverage (HJD)
1999 Jul 4–5	Keck/HIRES	3890–6270 in 35 orders	31.6	0.1	2,451,363–2,451,364
1999 Jul 21–23	Lick/Hamilton	3650–7675 in 81 orders	31.6	0.1	2,451,381–2,451,383
1999 Aug 21–23	Lick/Hamilton	3650–7675 in 81 orders	31.6	0.1	2,451,411–2,451,413
1999 Oct 14–15	Keck/HIRES	3700–5250 in 29 orders	31.6	0.1	2,451,466–2,451,467
2000 Jul 10–11	Lick/Hamilton	3650–7675 in 81 orders	31.6	0.1	2,451,736–2,451,737
2000 Sep 18–19	Keck/HIRES	3700–5250 in 29 orders	31.6	0.1	2,451,805–2,451,806
2001 Aug 24	WIYN/Hydra	3800–4490 in order 2	1200	0.9	2,452,146
2001 Sep 8–9	WIYN/Hydra	3800–4490 in order 2	1200	0.9	2,452,161–2,452,162
2004 Nov 28–30	WIYN/Hydra	3800–4490 in order 2	1200	0.9	2,453,338–2,453,340
2005 Jul 18–21	WIRO/WIRO-Spec	3800–4490 in order 1	2400	2.5	2,453,570–2,453,573
2005 Jul 18–20,22	WIRO/WIRO-Spec	3800–4490 in order 1	2400	2.5	2,453,632–2,453,635
2005 Oct 13	WIRO/Longslit	4050–6050 in order 2	600	2.5	2,453,657
2006 Jun 16–20	WIRO/Longslit	3900–5900 in order 2	600	2.5	2,453,903–2,453,907
2006 Jul 15–16,20	WIRO/Longslit	3900–5900 in order 2	600	2.5	2,453,932–2,453,935
2006 Sep 8–11	WIYN/Hydra	3800–4490 in order 2	1200	0.9	2,453,987–2,453,990
2006 Oct 7	WIRO/Longslit	3900–5900 in order 2	600	2.5	2,454,016
2007 Jun 28–30	WIRO/Longslit	3900–5900 in order 2	600	2.5	2,454,280–2,454,282
2007 Jul 4–6	WIYN/Hydra	3820–4510 in order 2	1200	0.9	2,454,285–2,454,287
2007 Aug 28–Sep 4	WIRO/Longslit	5550–6850 in order 1	1800	1.5	2,454,341–2,454,348

Table 2. Orbital Elements

Element	MT059	MT258	Schulte 3	MT252	MT771
$P$ (Days)	4.8527 (0.0002)	14.660 (0.002)	4.7464 (0.0002)	18–19	1.5:
$e$	0.11 (0.04)	0.03 (0.05)	0.070 (0.009)	...	...
$\omega$ (deg)	212 (17)	68 (71)	5.5 (0.7)	...	...
$\gamma$ (km s <sup>-1</sup> )	-24.2 (1.7)	-20.8 (1.2)	-26.4 (1.7)	-18 (10)	-36 (10)
$T_0$ (HJD-2,400,000)	53916.72 (0.22)	53922.03 (2.87)	53987.81 (0.01)	54341.9 (1.0)	54343.8 (0.5)
$K_1$ (km s <sup>-1</sup> )	72.3 (2.3)	41.2 (1.7)	113.2 (14.5)	85 (13)	124 (13)
$K_2$ (km s <sup>-1</sup> )	...	...	256.7 (2.4)	107 (13)	153 (14)
$M_1$ (M <sub>⊙</sub> )	21.4 (0.6) <sup>a</sup>	21.4 (0.6) <sup>a</sup>	> 17.2 (0.3)	> 8 ± 1	> 1.8 (0.2)
$M_2$ (M <sub>⊙</sub> )	5.1 (0.3)–13.8 (0.6)	4.1 (0.2)–17.5 (1.0)	> 7.6 (1.4)	> 6 ± 1	> 1.5 (0.2)
$f(m)_1$ (M <sub>⊙</sub> )	0.187 (0.018)	0.106 (0.013)	0.709 (0.273)	...	...
$f(m)_2$ (M <sub>⊙</sub> )	...	...	8.289 (0.237)	...	...
S. C. <sub>1</sub>	O8V	O8V	O6IV:	B1.5III	O7V
S. C. <sub>2</sub>	B	B	O9III	B1V	O9V
$a_1 \sin i$ (R <sub>⊙</sub> )	6.9 (0.2)	11.9 (0.5)	7.4 (0.9)	22 (3)	2.6 (0.3)
$a_2 \sin i$ (R <sub>⊙</sub> )	...	...	16.7 (0.2)	27 (3)	3.2 (0.3)
$rms_1$ (km s <sup>-1</sup> )	11.0	6.7	38.7	...	...
$rms_2$ (km s <sup>-1</sup> )	...	...	9.0	...	...

Note. — Calculated errors are located in parentheses.

<sup>a</sup>Theoretical masses adopted from Martins et al. (2005).



Table 3. Ephemerides for MT059 & MT258

Star	Date (HJD-2,400,000)	$\phi$	$V_r$ (km s <sup>-1</sup> )	1 $\sigma$ err (km s <sup>-1</sup> )	$O - C$ (km s <sup>-1</sup> )
MT059...	51381.50	0.562	10.0	25.6	-5.8
	51411.50	0.744	-89.1	31.6	-37.2
	51413.50	0.156	-4.0	15.4	15.4
	51467.91	0.369	51.8	13.4	11.2
	51736.50	0.717	-32.4	32.8	8.2
	51737.50	0.924	-98.0	14.6	5.2
	51805.75	0.988	-106.7	6.0	-10.5
	52146.70	0.248	15.7	4.1	-2.7
	52162.66	0.538	26.9	4.4	4.7
	53338.62	0.871	-90.3	4.7	6.1
	53570.50	0.654	-26.3	5.2	-11.3
	53571.50	0.860	-103.3	5.2	-9.4
	53573.50	0.272	21.3	5.1	-4.3
	53633.50	0.637	-15.6	4.9	-7.1
	53634.50	0.843	-88.6	5.0	0.4
	53636.50	0.255	26.4	5.6	5.6
	53657.50	0.582	34.7	4.3	24.7
	53903.72	0.322	28.3	15.6	-7.6
	53903.73	0.324	24.3	11.1	-11.9
	53903.74	0.325	32.6	11.0	-3.7
	53903.84	0.346	37.0	11.5	-1.8
	53903.84	0.347	39.1	12.0	0.0
	53904.70	0.523	5.7	11.6	-20.0
	53904.71	0.525	35.0	11.5	9.6
	53904.86	0.558	7.0	11.1	-10.1
	53904.89	0.563	22.9	11.0	7.1
	53905.74	0.739	-82.5	13.8	-33.0
	53905.82	0.755	-53.0	11.0	3.4
	53905.84	0.758	-48.6	10.9	9.1
	53906.72	0.939	-99.7	12.1	3.4
	53906.72	0.941	-100.0	11.4	3.1
	53906.87	0.972	-112.8	11.7	-13.1
	53907.77	0.156	-22.4	11.1	-2.7
	53907.86	0.175	-10.3	11.0	0.0
	53932.73	0.301	42.1	11.0	9.9
	53932.83	0.321	77.8	13.3	42.0
	53932.84	0.322	67.8	12.4	31.8
	53935.77	0.927	-91.2	13.2	12.1
	53935.85	0.943	-71.5	12.0	31.4
	53987.70	0.628	-1.2	8.3	3.8
	53988.74	0.843	-79.0	6.3	10.0
	53989.66	0.031	-82.7	4.2	-0.9
	53990.85	0.277	30.2	5.1	3.2
	54285.93	0.084	-48.9	6.4	8.0
MT258...	51467.91	0.262	-11.4	7.7	1.3

Table 3—Continued

Star	Date (HJD-2,400,000)	$\phi$	$V_r$ (km s <sup>-1</sup> )	1 $\sigma$ err (km s <sup>-1</sup> )	$O - C$ (km s <sup>-1</sup> )
	51805.74	0.223	1.4	4.8	3.5
	52146.70	0.386	21.7	3.9	6.0
	52161.81	0.368	12.2	3.8	1.3
	52162.66	0.424	-1.7	3.8	0.1
	53338.62	0.867	-44.4	3.6	9.7
	53340.59	0.995	-57.4	4.0	3.0
	53571.50	0.005	-36.3	4.4	-7.1
	53573.50	0.135	-57.2	4.5	-0.1
	53632.50	0.970	-62.0	6.3	-2.4
	53633.50	0.035	-72.8	4.7	-11.5
	53903.76	0.603	12.5	11.1	-4.8
	53903.77	0.604	13.3	11.3	-4.1
	53904.76	0.668	11.9	11.0	-9.0
	53904.77	0.668	10.3	11.6	-10.5
	53906.75	0.797	-4.1	11.0	-9.0
	53906.76	0.798	1.7	11.2	-3.1
	53906.76	0.798	-5.6	11.1	-10.3
	53907.81	0.867	-17.7	10.7	-4.5
	53907.82	0.867	-12.6	10.8	0.6
	53932.75	0.488	11.3	10.9	-3.3
	53932.86	0.495	34.9	11.1	19.2
	53935.81	0.686	5.3	12.6	-3.3
	53935.86	0.690	19.6	11.5	11.6
	53987.70	0.060	-38.5	4.6	1.5
	53988.74	0.127	-17.0	4.4	6.5
	53989.66	0.187	-13.2	3.7	-4.7
	53989.78	0.195	-11.3	4.2	-4.7
	53990.85	0.264	8.2	4.3	-0.6
	54285.93	0.446	19.3	4.0	-1.6
	54286.66	0.493	21.2	5.7	2.7
	54342.88	0.708	10.9	13.6	-0.1
	54343.76	0.768	23.9	14.0	5.1
	54345.82	0.908	22.0	13.8	7.7
	54347.81	0.044	-6.7	13.6	10.0

Table 4. Ephemerides for Schulte 3, MT252, & MT771

Star	Date (HJD-2,400,000)	$\phi$	$V_{r1}$ (km s <sup>-1</sup> )	$O_1 - C_1$ (km s <sup>-1</sup> )	$V_{r2}$ (km s <sup>-1</sup> )	$O_2 - C_2$ (km s <sup>-1</sup> )
Schulte 3.....	53987.69	0.974	-111 (20)	35.4	250 (8)	2.9
	53988.74	0.195	12 (20)	63.7	13 (8)	-7.7
	53989.65	0.387	78 (20)	17.0	-224 (8)	6.1
	53989.77	0.412	46 (20)	-22.6	-244 (8)	2.2
	53990.85	0.639	90 (20)	47.9	-179 (8)	-5.1
	54285.93	0.809	-123 (20)	-56.1	91 (8)	15.8
	54341.80	0.580	112 (20)	46.7	-229 (8)	0.3
	54342.72	0.773	-10 (20)	31.6	12 (8)	-6.6
	54343.83	0.007	-139 (20)	7.7	243 (8)	-2.2
	54344.76	0.203	-20 (20)	25.5	13 (8)	6.5
	54345.78	0.418	73 (20)	2.7	-257 (8)	-7.4
	54346.79	0.631	69 (20)	23.1	-179 (8)	3.9
	54347.75	0.833	-41 (20)	42.9	103 (8)	-10.3
	54348.84	0.063	-125 (20)	8.0	211 (8)	0.9
MT252.....	54341.85	...	67 (8)	...	-125 (8)	...
	54342.84	...	1:	...	-83:	...
	54343.79	...	-9:	...	...	...
	54345.85	...	-27:	...	...	...
	54346.88	...	-63:	...	...	...
MT771.....	54348.78	...	-64:	...	41:	...
	54341.81	...	63 (10)	...	-165 (10)	...
	54342.81	...	...	...	-11:	...
	54343.82	...	88 (8)	...	-189 (10)	...
	54345.83	...	-36 (10)	...	-36 (10)	...
	54347.82	...	...	...	89:	...
	54348.77	...	...	...	-26:	...

Table 5. OB Binaries in Cyg OB2

Star	Type	S.C.	P (days)	q	Ref.
MT059	SB1	O8V & B	4.8527 (0.0002)	0.24 (0.02)–0.64 (0.03)	1
MT252	SB2	B2III & B1V	18–19	0.8 (0.02)	1
MT258	SB1	O8V & B	14.660 (0.002)	0.19 (0.01)–0.84 (0.05)	1
MT421	EA	O9V & B9V–A0V	4.161	...	2
MT429	EA	B0V & ??	2.9788	...	2
MT696	EW/KE	O9.5V & early B	1.46	...	3
MT720	SB2	early B & early B	< 5	...	1
MT771	SB2	O7V & O9V	1.5:	0.8 (0.1)	1
Schulte 3	SB2/EA:	O6IV: & O9III	4.7464 (0.0002)	0.44 (0.08)	1,4
Schulte 5	EB	O7Ianf & Ofpe/WN9 (& B0V?)	6.6	0.28 (0.02)	5,6,7,8,9,10
Schulte 8a	SB2	O5.5I & O6:	21.908	0.86 (0.04)	11,12

Note. — Photometric types EW/KE, EA, and EB stand for Contact system of the W UMa type (ellipsoidal;  $P < 1$  day), Algol type (near spherical), and  $\beta$  Lyr type (ellipsoidal;  $P > 1$  day) respectively.

References. — (1) This study; (2) Pigulski & Kolaczowski (1998); (3) Rios & DeGioia-Eastwood (2004); (4) Kinemuchi et al. (2008, in prep); (5) Wilson (1948); (6) Wilson & Abt (1951); (7) Miczaika (1953); (8) Walborn (1973); (9) Contreras et al. (1997); (10) Rauw et al. (1999); (11) Romano (1969); (12) De Becker et al. (2004)

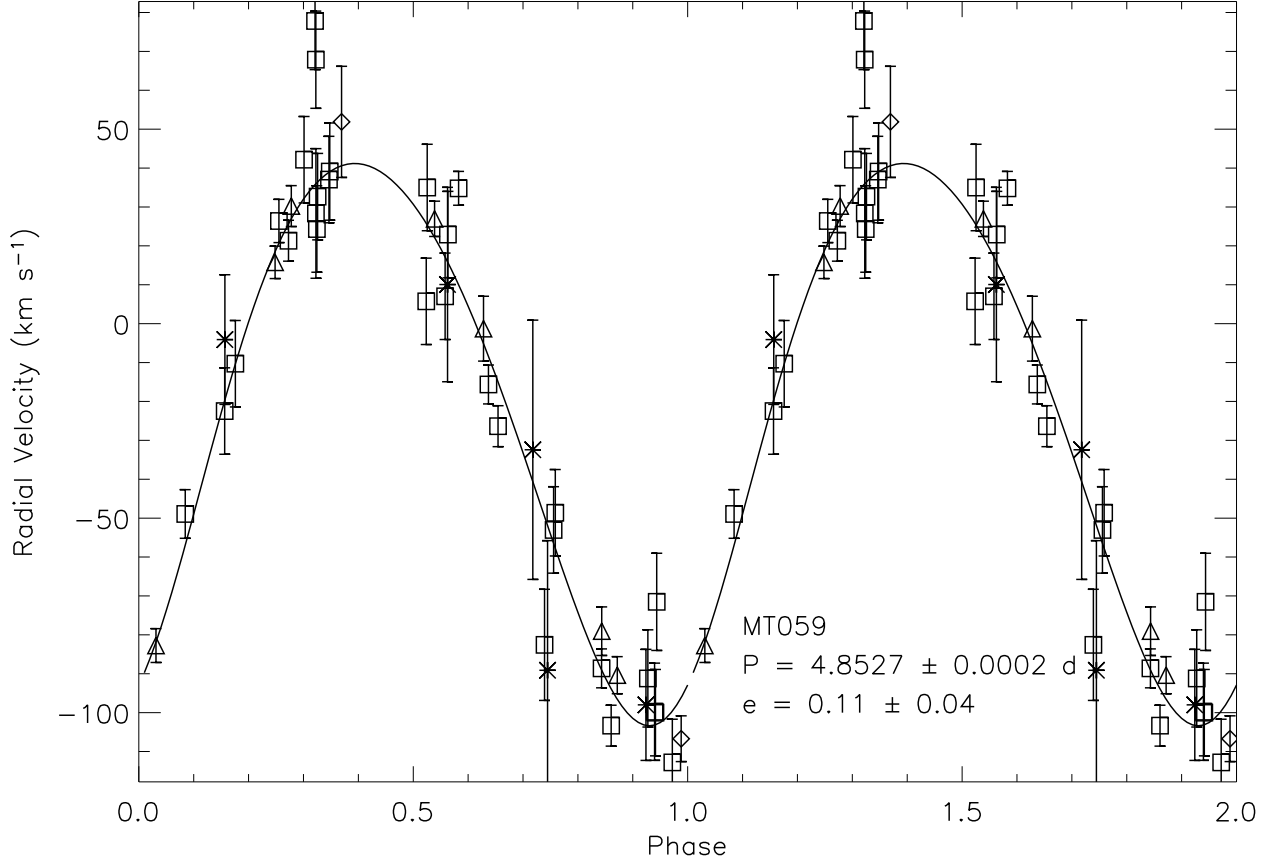


Fig. 1.—  $V_r$  curve and orbital solution to the O8V star, MT059. The symbols correspond to the different observatories, where the stars are observations taken with the Hamilton Spectrograph (Lick), the diamonds are observations taken with HIRES (Keck), the triangles are observations taken with Hydra (WIYN), and the squares are observations taken with WIROspec or the Longslit Spectrograph (WIRO).

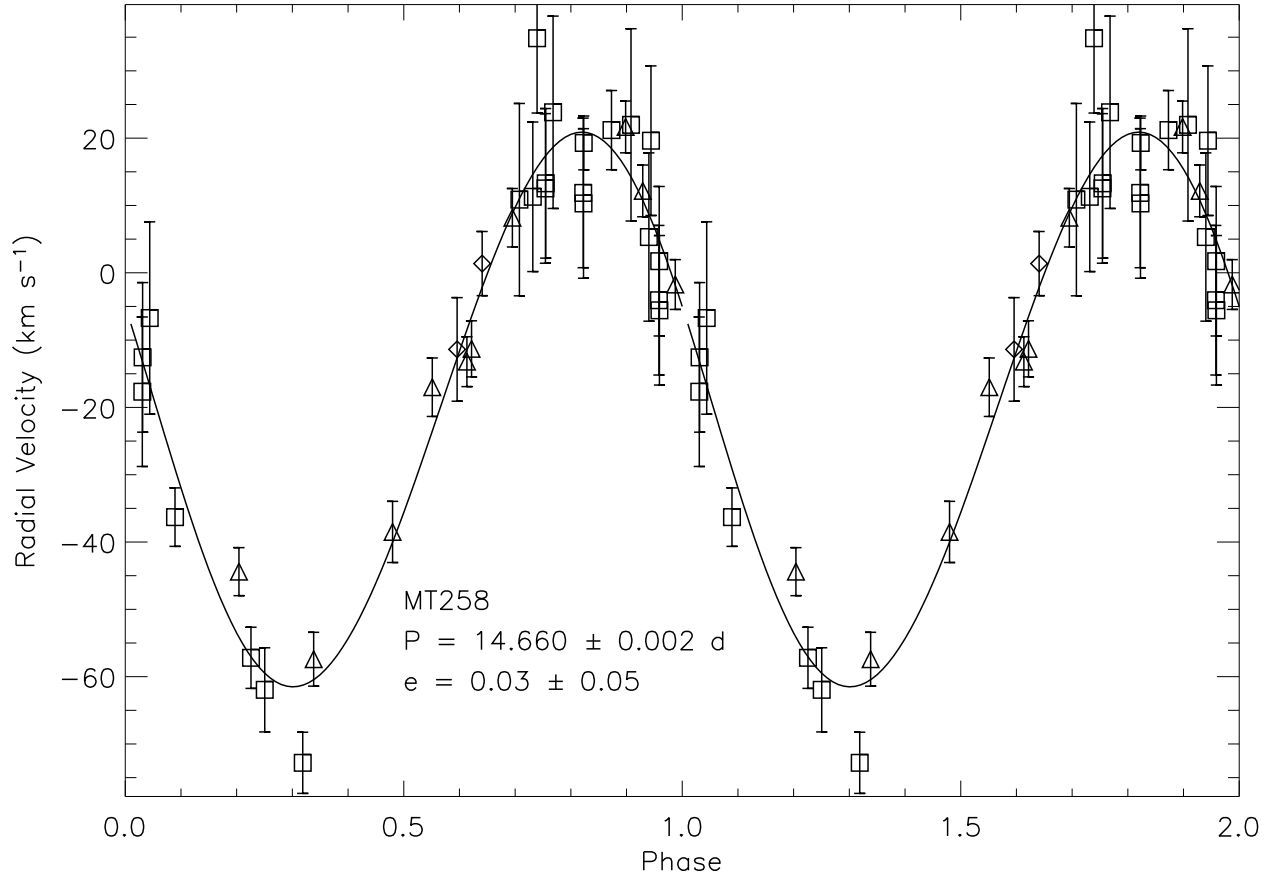


Fig. 2.—  $V_r$  curve and orbital solution to the O8V star, MT258 using the same format as Figure 1.

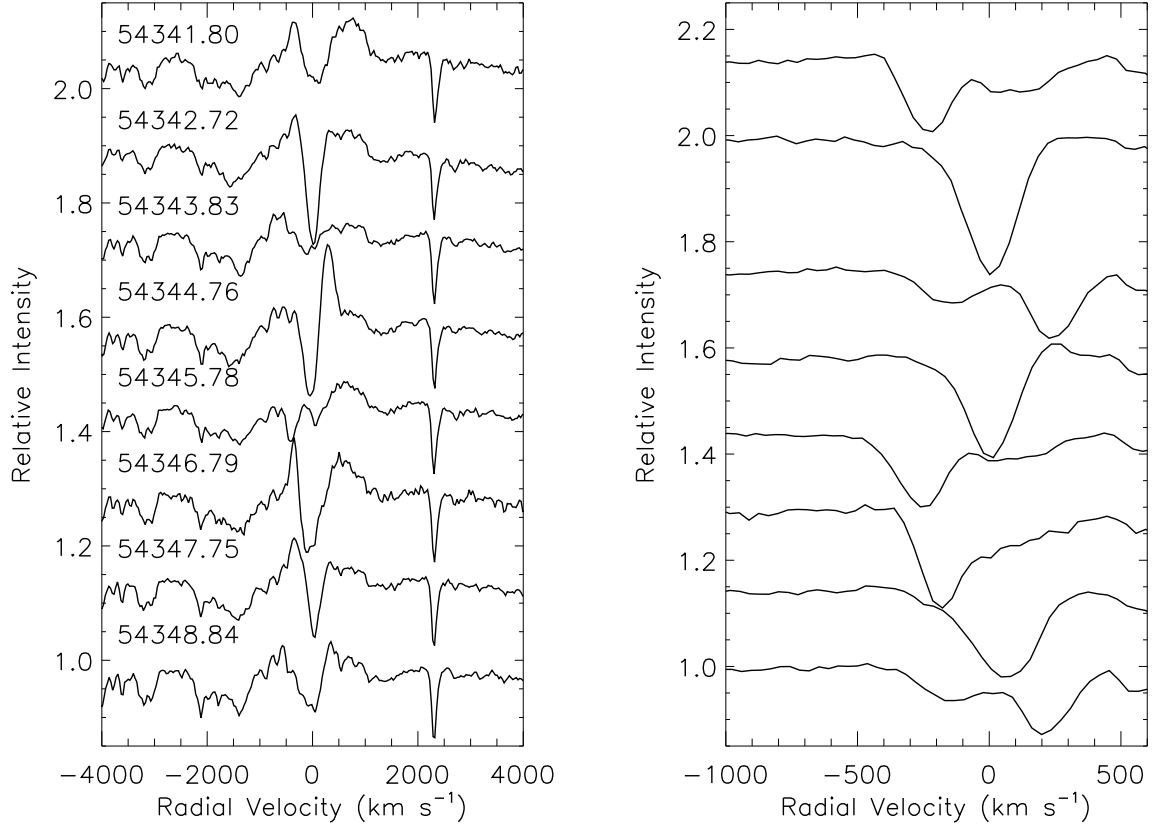


Fig. 3.— H $\alpha$   $\lambda 6562.80$  Å (left) and He I  $\lambda 5875.75$  Å (right) in velocity space for Schulte 3 between 2007 August 28 and 2007 September 4. Dates are listed as HJD - 2,400,000 and apply to both left and right panels.

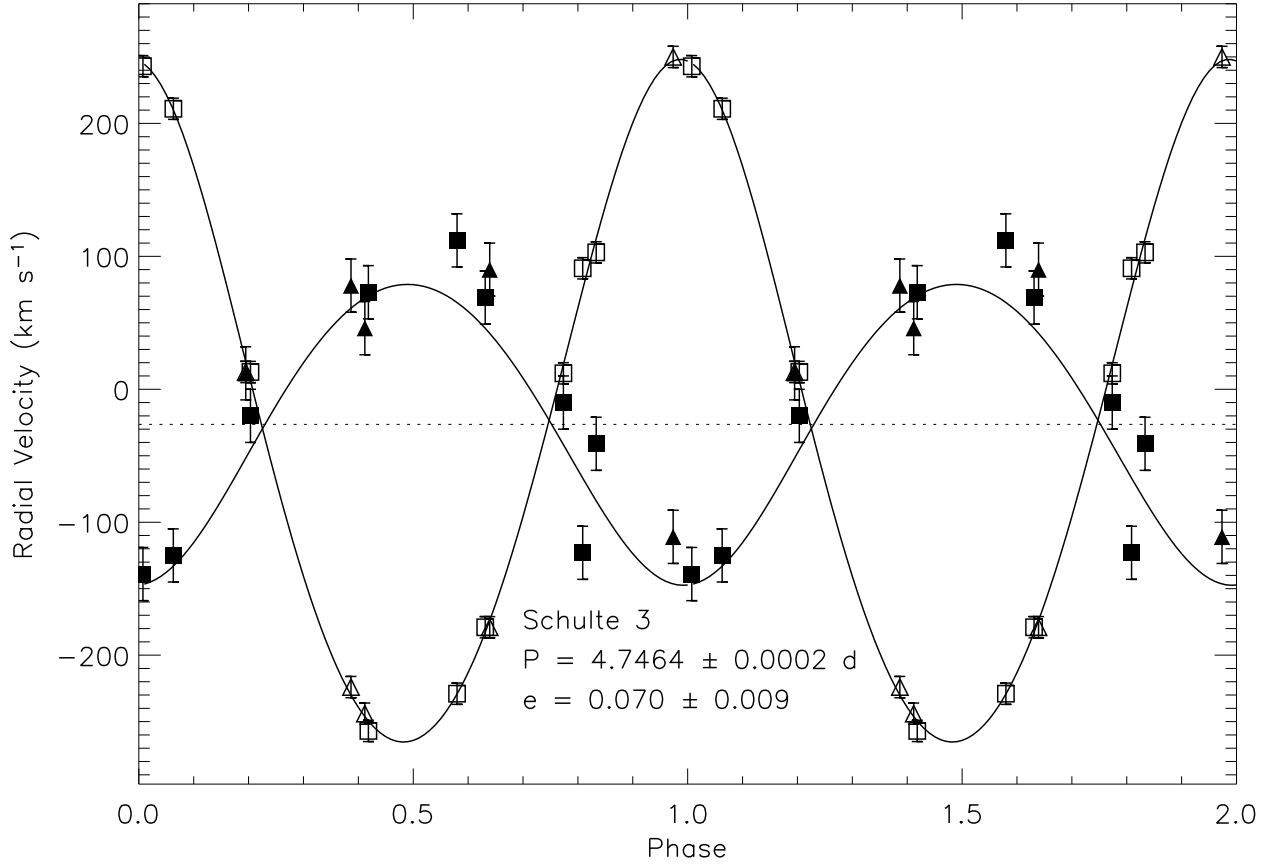


Fig. 4.—  $V_r$  curve and orbital solution for Schulte 3 using 14 of the 18 observations. The filled points correspond to the primary (O6IV:) and the unfilled points correspond to the secondary (O9III). The symbols represent the same observation locations as Figure 1.



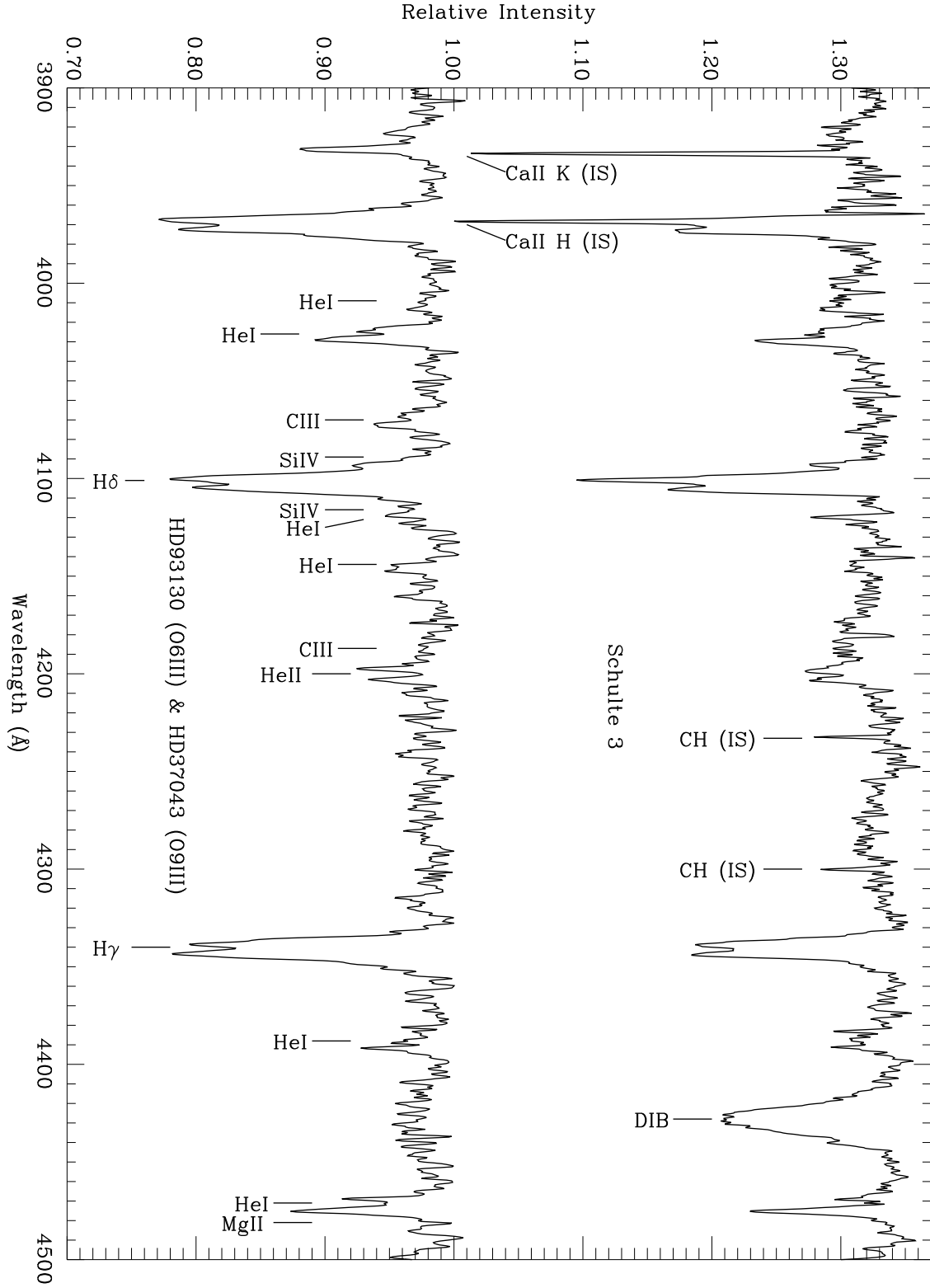


Fig. 5.— A spectrum of Schulte 3 obtained on 2007 July 5 with WIYN (top), and a composite of two shifted spectra from the Walborn & Fitzpatrick (1990) digital atlas (bottom) that best match the spectral types of the primary and secondary of Schulte 3. The primary is shifted  $-110 \text{ km s}^{-1}$  and the secondary is shifted  $257 \text{ km s}^{-1}$ . Absorption features are labeled at their respective intrinsic values.

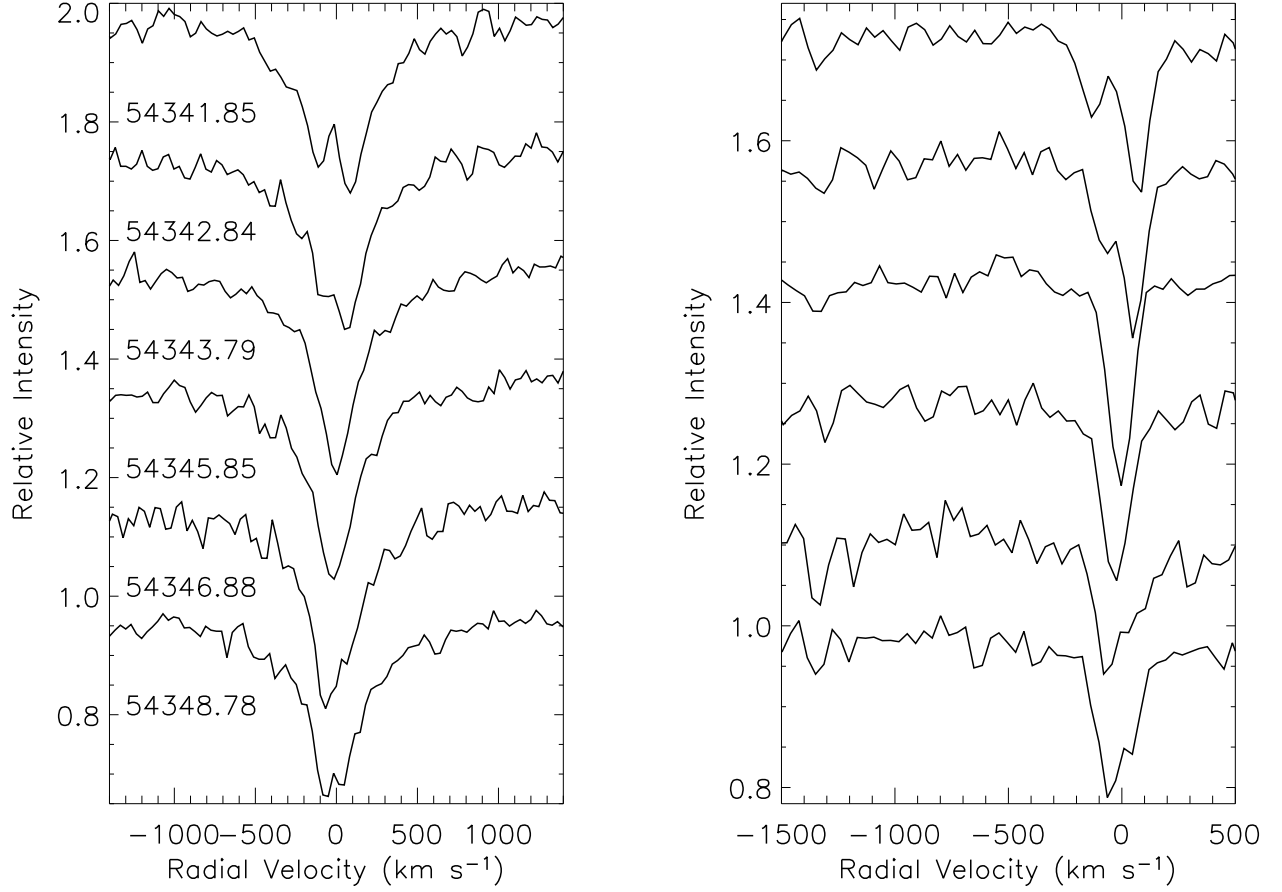


Fig. 6.— H $\alpha$   $\lambda 6562.80$  Å and He I  $\lambda 5875.75$  Å absorption in velocity space for MT252 using same format as Figure 3.

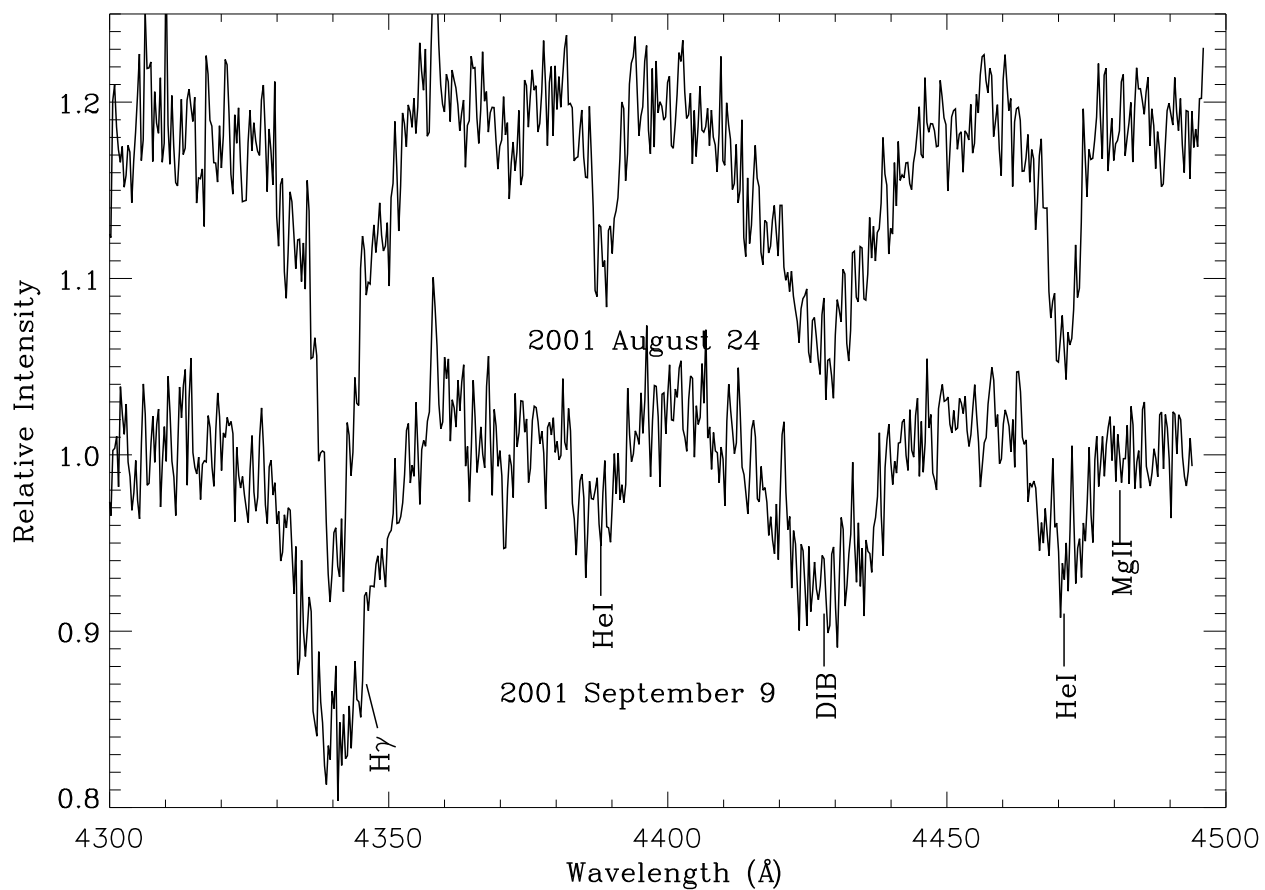


Fig. 7.— A portion of the 2001 August 24 (top) and 2001 September 9 (bottom) spectra for MT720, showing the nearly blended and unblended states respectively.

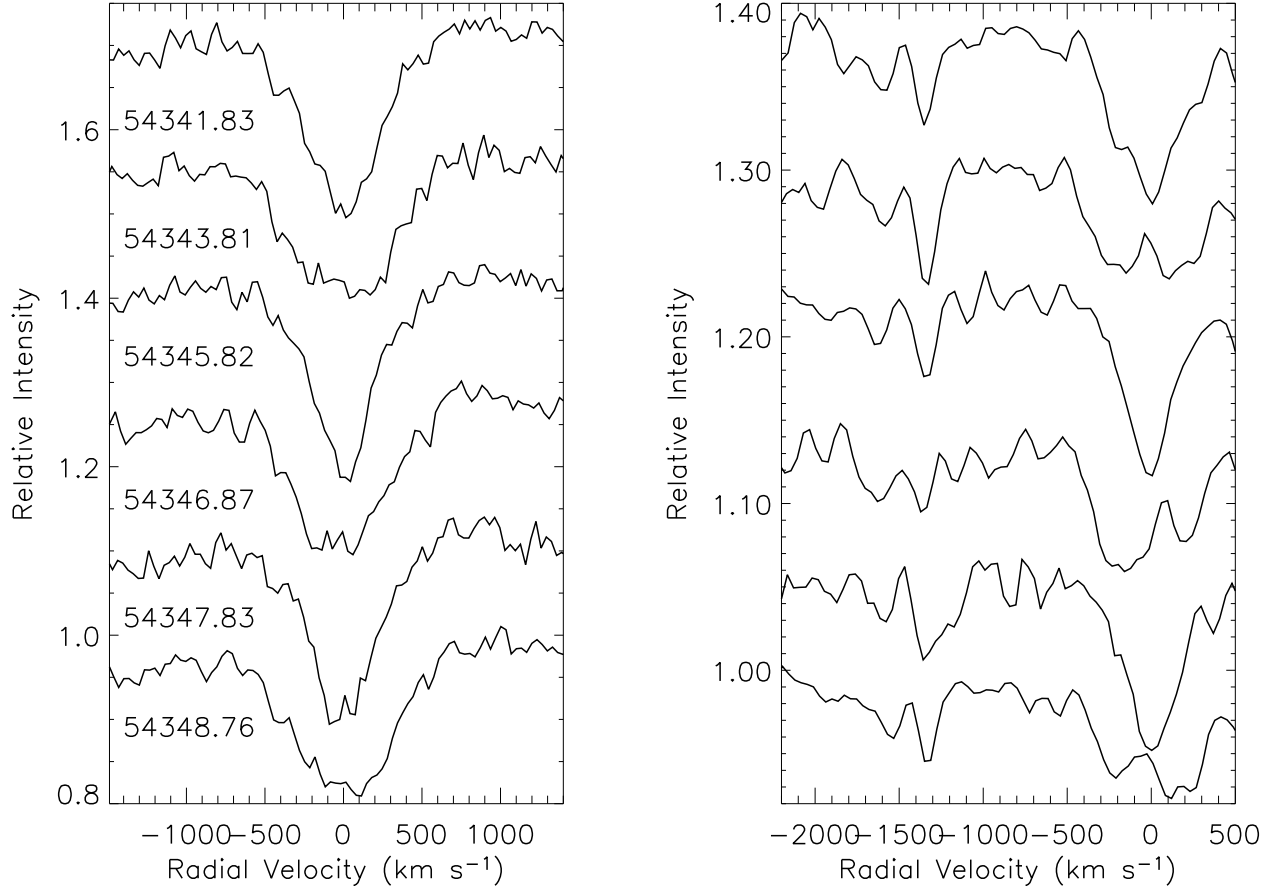


Fig. 8.— H $\alpha$   $\lambda 6562.80$  Å and He I  $\lambda 5875.75$  Å absorption in velocity space for MT720 using same format as Figure 3.

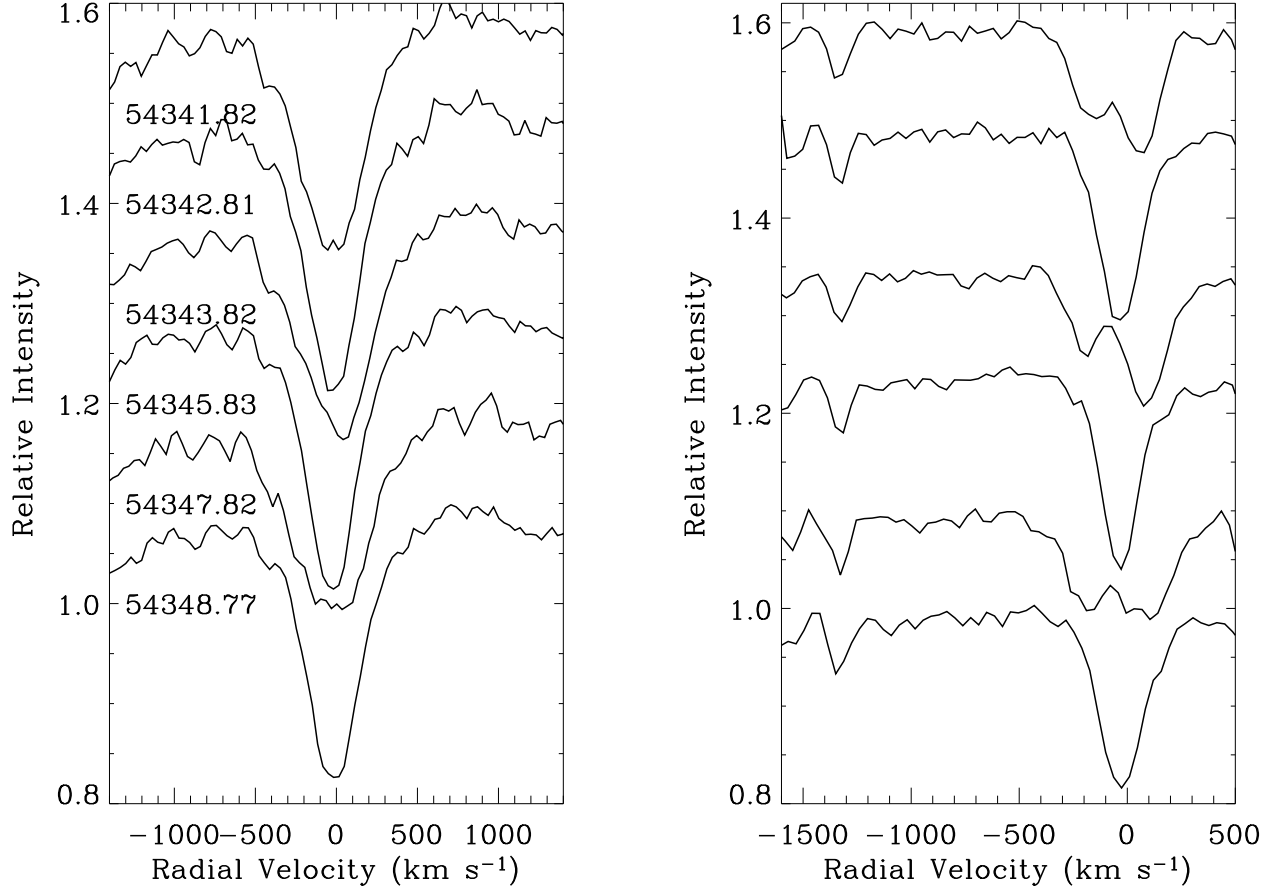


Fig. 9.— H $\alpha$   $\lambda 6562.80$  Å and He I  $\lambda 5875.75$  Å absorption in velocity space for MT771 using same format as Figure 3.

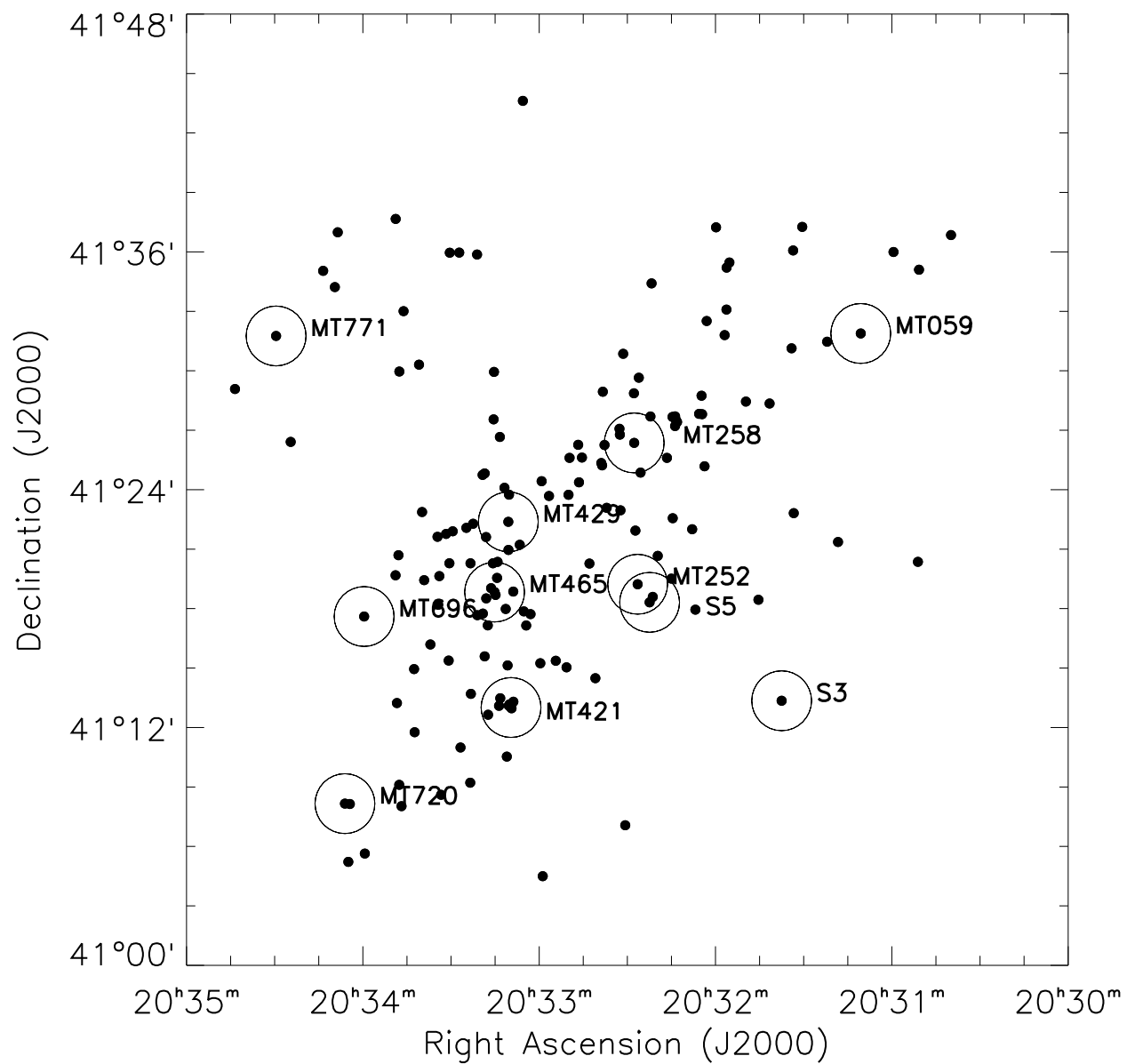


Fig. 10.— A map of OB stars from this survey. Circles indicate the location of known OB binaries within this region of Cyg OB2.